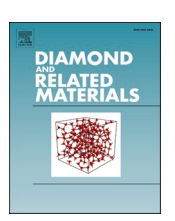
ELSEVIER

Contents lists available at ScienceDirect

Diamond & Related Materials

journal homepage: www.elsevier.com/locate/diamond





Novel superhard BC₁₀N synthesized by microwave plasma CVD

Kallol Chakrabarty, Paul A. Baker, Shane A. Catledge

The University of Alabama at Birmingham, Dept. of Physics, 1720 2nd Ave. S., ESH 4100, Birmingham, AL 35294-1170, United States of America

ARTICLE INFO

Keywords:
Microwave plasma CVD
XPS
XRD
FTIR
Superhard
Coating

ABSTRACT

Microwave Plasma Chemical Vapor Deposition (MPCVD) was used to synthesize novel superhard $BC_{10}N$ on silicon substrates. Feedgas mixtures of H_2 , CH_4 , N_2 , and B_2H_6 were used for a range of systematically varied microwave power, chamber pressure, and flow rate conditions. Optical Emission Spectroscopy (OES) was used to guide the synthesis of $BC_{10}N$. Plasma optical emission from the C_2 peak increases with pressure up to 80 Torr and saturates in the 80-100 Torr range. The C_2 emission also follows the same trend, growing non-linearly with increasing microwave power (for fixed chamber pressure of 30 Torr). The presence of abundant C_2 in the plasma is advantageous under specific growth conditions to produce superhard carbon-rich $BC_{10}N$, a material that has been theoretically predicted but not yet synthesized. Findings obtained from X-ray Photoelectron Spectroscopy (XPS) and Fourier Transform Infrared Spectroscopy (FTIR) elucidate the existence of B-C, C-N, B-N, and B-N-C bonding in the synthesized coating. Nanoindentation hardness measurements are within the superhard regime, showing an average hardness of 63 GPa.

1. Introduction

The wide range of industrial applications, including cutting, polishing, and protective coatings, has led to a significant focus on the design and synthesis of new superhard materials. This attention stems from the desire to develop materials with exceptional hardness and wear resistance, enhancing efficiency and durability in various industrial processes [1]. Diamond, renowned as the hardest known material with a hardness value ranging from 70 to 100 GPa, exhibits noteworthy properties such as thermal insulation and electrical conductivity, but it also has some significant limitations. The high cost of the diamond, coupled with its susceptibility to oxidation at temperatures exceeding 800 °C and constraints in efficiently machining ferrous alloys due to chemical interactions with iron group elements, limit its practical applicability [2-4]. Therefore, diamond's high cost and unsuitability for numerous applications prompt exploration of new novel superhard materials. Materials within the 'CNOB' system, comprised of the light elements carbon, nitrogen, oxygen, and boron, emerge as promising alternatives and contain some of the hardest known materials. The light elements in the 'CNOB' system possess the ability to form short bond lengths and exhibit a propensity for creating directional covalent bonds. These structural characteristics render the formations resistant to compression or distortion [5-7]. Over the past few years, considerable interest has been in the B-C-N ternary system and its superhard phases. Ternary boron carbonitride (B_xC_vN_z) coatings have gathered significant attention due to their unique combination of boron, carbon, and nitrogen elements, which offer the potential for exceptional mechanical, thermal, and chemical properties. Numerous investigations have been carried out to explore the B-C-N phase system [8-11]. Materials within the B-C-N system are distinguished by their short bond lengths and are expected to exhibit a combination of specific properties found in boron carbide (B₄C), hexagonal boron nitride (h-BN), cubic boron nitride (c-BN), and diamond [5]. These properties include low friction coefficient, excellent wear resistance, high hardness, and superior thermal and chemical stability. Due to their impressive properties, materials within the B-C-N system are regarded as promising candidates for applications requiring hard and protective coatings, particularly for cutting tools and other wear-resistant purposes. Moreover, the wide composition range achievable in B_xC_vN_z coatings makes them well-suited for electronic and photonic devices, optical and optoelectronics applications, as well as rechargeable lithium batteries [12,13]. Several methods have been utilized to synthesize phases within the ternary system of boron, carbon, and nitrogen, employing different atomic compositions. These methods include high pressure-high temperature (HPHT) synthesis [12], chemical vapor deposition (CVD) [14], plasma-assisted chemical vapor deposition (PACVD) [8,9], pulsed laser deposition [10,11], mixing and ball milling of graphite/h-BN powders [15], solid phase nitriding [16] and solid-state pyrolysis [17], ion beam deposition [18], as well as RF

E-mail address: catledge@uab.edu (S.A. Catledge).

 $^{^{\}ast}$ Corresponding author.

and DC sputtering [19,20].

Exploring novel superhard ternary materials poses challenges due to the extensive phase space resulting from numerous potential combinations of elements. Recently, Chen et al. have successfully predicted novel superhard ternary BC10N materials, calculating the bulk and shear moduli of approximately 10,000 existing compounds sourced from the Materials Project database [21]. This BC10N compound demonstrates dynamic stability (i.e., without negative phonon modes) and possesses relatively low formation energy. The compound BC10N exhibits a computed hardness of approximately 87 GPa, which is comparable to that of diamond. Consequently, it is anticipated to exhibit improved performance, especially in environments with elevated temperatures and humidity levels. Growth of the desired superhard structures via chemical vapor deposition (CVD) poses a significant challenge, often requiring optimization with only a narrow range of ideal conditions. The goal of this current work is the experimental validation of theoretical predictions of superhard ternary BC10N material. The chemistry prevailing in H₂/N₂/B₂H₆/CH₄ plasmas for ternary B-C-N synthesis is not well established. Key concerns regarding the gas-phase chemistry of these plasmas involve identifying crucial carbon/nitrogen/boroncontaining growth species, understanding their generation, and examining how discharge parameters such as power, pressure, and gas flow rate affect their densities and distributions. For synthesizing BC10N, growth species would likely contain boron, nitrogen, and carbon, as observed by optical emission spectroscopy. The objective of this study is to investigate the deposition conditions leading to the formation of theoretically predicted superhard BC10N coating via MPCVD, and to experimentally evaluate the structure and hardness of this compound.

2. Experimental details

2.1. In situ OES

Prior to the growth of any coatings, the optical emission spectroscopy of $\rm H_2/N_2/B_2H_6/CH_4$ plasmas was studied. Hydrogen (H_2) was used as the carrier gas along with diborane (as a mixture of 95 % H_2, 5 % B_2H_6 with ppm carbon), N_2, and CH_4. The gas flow rates were: 500 standard cubic centimeters per minute (sccm) of hydrogen, 5 sccm of the diborane mixture, 5 sccm of N_2 and 25 sccm of CH_4. Microwave power and chamber pressure were systematically varied to study the plasma's excited species. The OES data were collected using an Acton Research SpectraPro 500i spectrograph (Princeton Instruments, Trenton, NJ, USA) equipped with a 1200g/mm grating blazed at 300nm, and the entrance slit was adjusted to 20µm.

2.2. Sample preparation, synthesis and characterization

Microwave plasma chemical vapor deposition (MPCVD) system (Wavemat Inc. Plymouth, MI, USA) was used to synthesize Boron carbonitride ($B_x C_y N_z$) coatings, additional details of MPCVD will be found elsewhere [22,23]. A 525 μm thick N-type (100)-oriented silicon substrate was positioned on top of a 0.5" diameter molybdenum screw located along the central axis of the quartz bell jar. Before deposition, the substrate underwent ultrasonic cleaning with acetone, methanol, and distilled water. Before the deposition process, the substrate underwent mechanical seeding with diamond powder (particle size: 0–1 μm) on a polishing cloth for 90 s, followed by another round of ultrasonic cleaning with acetone, methanol, and distilled water.

The experiment was conducted at microwave power 1.6 kW and at a fixed chamber pressure of 30 Torr. Hydrogen (H_2) was used as the carrier gas while methane, nitrogen and diborane (mixture of 95 % H_2 , 5 % B_2H_6 ,) were used as the reactive gas. The gas flow rates were set at 500 Standard Cubic Centimeters per Minute (SCCM) of hydrogen, 25 SCCM of methane, 5 SCCM of nitrogen, and 5 SCCM of the diborane mixture. The $B_xC_yN_z$ coatings were synthesize at the average substrate temperature of 825 $\pm25~^{\circ}\text{C}$

The borocarbonitride samples were characterized employing various techniques including X-ray photoelectron Spectroscopy (XPS), Fourier Transformed Infrared Spectroscopy (FTIR), Raman Spectroscopy, Photoluminescence Spectroscopy, Grazing incidence X-ray diffraction (XRD), and Nanoindentation. The X-ray photoelectron spectroscopy (XPS) setup utilized in this study was a Phi Electronics VersaProbe 5000, featuring a micro-focused Al monochromatic source ($\lambda = 1486.6 \text{eV}$) and a dual anode conventional x-ray source equipped with a neutralizer. Survey spectra were taken with a step size of 0.8 eV and pass energy of 187.85 eV and the high resolution scans were a step size of 0.1 eV with pass energy of 23.5 eV. The C1s peak at 284.6 eV was considered the standard, and all hi-res spectra were calibrated and fitted accordingly. The attenuated total reflectance (ATR) mode of a Bruker Alpha FTIR spectrometer (Bruker Corporation, Billerica, MA, USA) was used to record FTIR spectra. A total of 1024 scans with a scan resolution of 4 cm⁻¹ were performed in the FTIR instrumentation to capture the entire spectrum. Raman spectra were recorded using a micro-Raman spectrometer (Dilor XY, Lille, France) equipped with a 532nm laser, a 1200groove/mm grating, and a 100× microscope objective. The same instrument was used for photoluminescence spectroscopy, but using a 600 g/mm grating. For X-ray diffraction (XRD) analysis, a Panalytical Empyrean X-ray diffractometer with Copper $K\alpha$ radiation (λ = 1.54059Å) was employed. The XRD patterns were acquired through a glancing-angle 2-theta scan with a 1° angle of incidence. The diffraction optics included a hybrid monochromator with a 1/8° divergence slit, a 1/16° anti-scattering slit, and a parallel plate collimator on the diffracted beam path with a proportional detector. HighScore Plus (version 4.8) was utilized for phase structure analysis, and Rietveld refinement was applied to determine the lattice constants of each sample. Nanoindentation hardness measurements were conducted using the Agilent Nano Indenter G200 (MTS Nano Instruments, Oak Ridge, TN, USA) equipped with a Berkovich diamond tip having a nominal radius of 50 nm. To calibrate the instrument, a fused silica reference with an accepted Young's modulus value of 72 GPa was evaluated both before and after indenting our sample. The stability of the diamond tip's shape during the sample examination was confirmed by comparing Young's modulus range of the silica standard before and after indenting our sample. The consistent range of Young's modulus 72 \pm 3 GPa for the silica standard, observed before and after indentation, indicates that the tip shape remained unchanged throughout the examination. All indents, including those made on the silica reference, were created to a maximum depth of 300 nm. Hardness measurements were determined at the maximum load applied during the indentation process.

3. Results

3.1. Optical emission spectroscopy (OES)

As our goal was to synthesize $BC_{10}N$, which is a carbon-rich B-C-N ternary material, our main focus was on the generation and behavior of the C_2 peak. A systematic variation of microwave power and chamber pressure was carried out to investigate the trends of the C_2 peak in the plasma. Fig. 1(a) shows that the normalized intensity of the C_2 peak increases non-linearly with increasing chamber pressure (for fixed microwave power of 1.6 kW). The C_2 peak intensity increases until 80 Torr and saturates in the range 80–100 Torr. Fig. 1(b) shows that the normalized intensity of the C_2 peak also follows the same trend and increases non-linearly with increasing microwave power (for a fixed chamber pressure of 30 Torr). These results suggest that higher microwave power and higher chamber pressure can be beneficial to provide the carbon-rich plasma environment needed for $BC_{10}N$ deposition.

3.2. X-ray photoelectron spectroscopy of borocarbonitride $(B_xC_yN_z)$

XPS of the borocarbonitride $(B_xC_yN_z)$ coating synthesized at microwave power 1.6 kW and at fixed chamber pressure of 30 Torr revealed

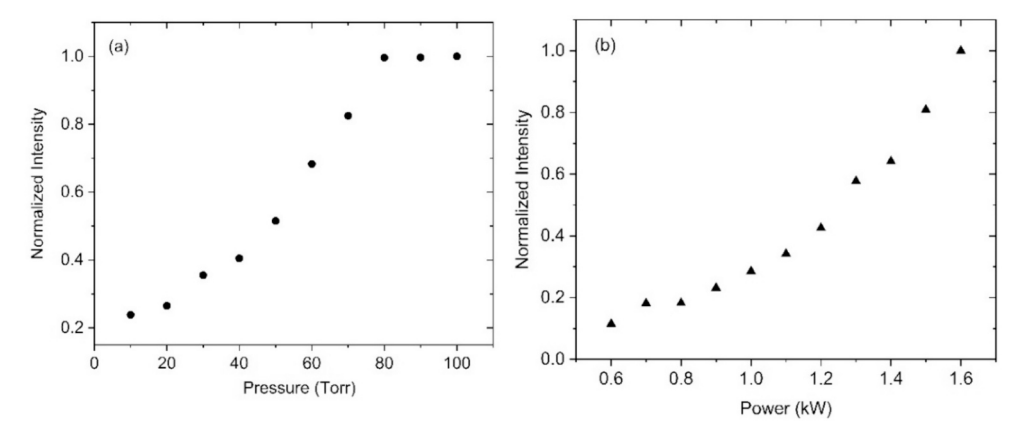


Fig. 1. (a) C_2 peak intensity ($\lambda = 517$ nm) for pressure range 20–100 Torr and fixed power of 1.60 kW (b) C_2 peak intensity for power range 0.6–1.6 kW at a fixed pressure of 30 Torr.

that the surface consists of 82 % carbon, 9.5 % boron, and 8.5 % nitrogen (relative atomic percentages), with no other elements detected. The true stoichiometric ratio for BC₁₀N would correspond to 83.3 % C, 8.3 % B, and 8.3 % N and are very close to the experimental survey spectra found here. The high-resolution XPS spectra of C1s, B1s, and N1s show C=C, C=N, C=B, and B=N bonding in the coating [24–27]. In Fig. 2(b), the high-resolution C1s scan indicates that 13 % of the carbon is bonded to boron (C=B), 44 % is involved in carbon-carbon double bonds (C=C), and the remaining 43 % is bonded to nitrogen (C=N). Fig. 2(c) displays the high-resolution B1s scan, revealing that 12 % of the boron is bonded to carbon (B=C), 60 % is bonded to nitrogen (B=N), and the remaining 28 % is involved in B-N-C bonding. Lastly, Fig. 2(d) presents the high-resolution N1s scan, illustrating that 69 % of the nitrogen is bonded to boron (N=B), while the remaining 31 % is bonded to carbon (N=C).

3.3. Fourier transform infrared spectroscopy (FTIR) of borocarbonitride $(B_x C_v N_z)$

Fig. 3 displays the FTIR spectrum of the borocarbonitride $(B_xC_yN_z)$ coating, showcasing multiple peaks within the fingerprint region (1500–500 cm $^{-1}$). These peaks indicate the presence of C=C, B=N, C=N, B=C, and B-N-C bonds within the synthesized coating, thus confirming its ternary nature as $B_xC_yN_z$. Especially, the intensity of the C=C peak is notably prominent, implying a carbon-rich composition of the ternary boron carbonitride. For a comprehensive understanding, the complete peak assignment is provided in Table 1.

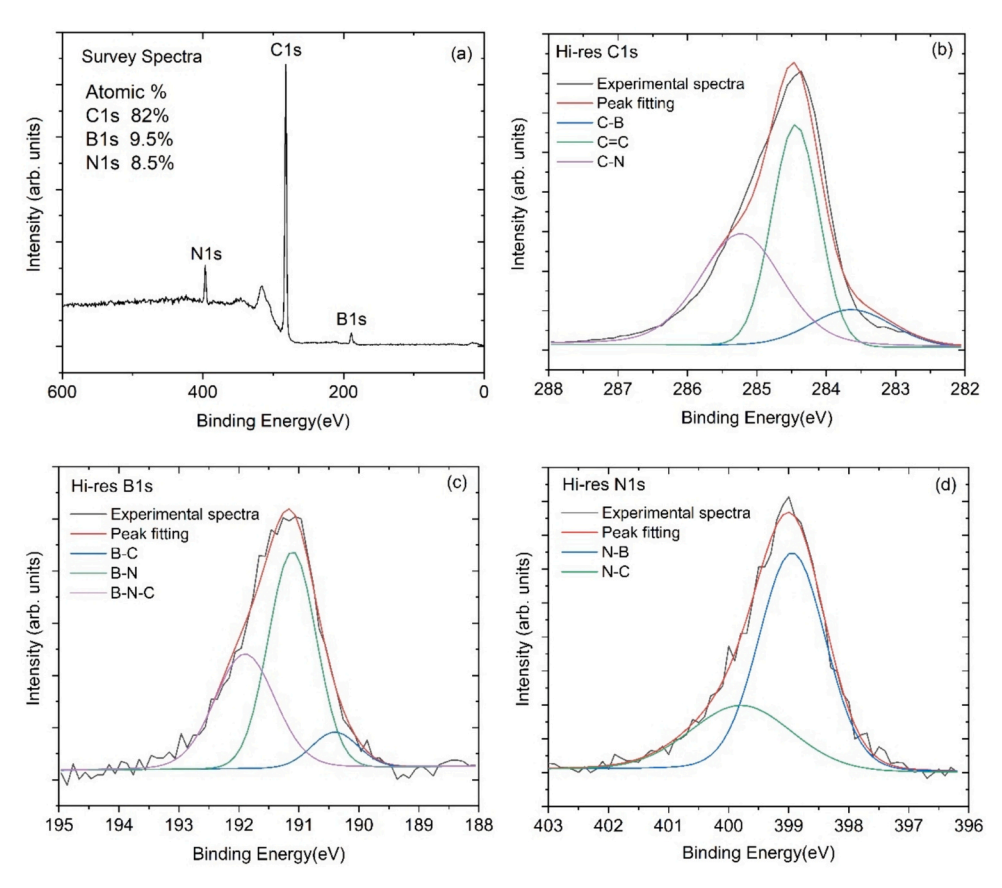


Fig. 2. (a) Survey spectra and high-resolution XPS spectra of (a) C1s, (b) B1s, and (c) N1s. Hi-res spectra show C=C, C-N, C-B, and B-N bonding in the coating.

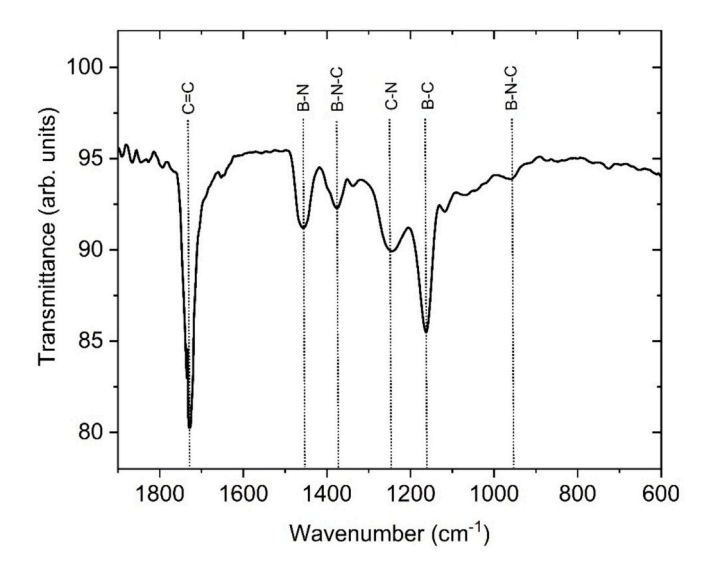


Fig. 3. FTIR spectral analysis of borocarbonitride $(B_xC_yN_z)$ coating containing B—N, B—C, C=C, and B-N-C stretching vibrations.

Table 1Brocarbonitride complete FTIR peak assignment.

Transmittance frequency (cm ⁻¹)	Assignment	References
954	B-N-C	[24,25]
1160	B-C	[26,28,29]
1248	C-N	[24,28]
1377	B-N-C	[24,26]
1455	B-N	[30,31]
1730	C=C	[28]

3.4. Micro Raman spectroscopy of borocarbonitride $(B_xC_yN_z)$

Fig. 4 shows the Raman spectrum of the borocarbonitride $(B_x C_y N_z)$ coating. It reveals two broad peaks at 476 cm⁻¹ and 1213 cm⁻¹ and one sharp peak at 1302 cm⁻¹. The two broad peaks correspond to the borondoped diamond signature [32,33]. The peak at 1302 cm⁻¹ is the diamond peak. The shift of the diamond peak towards lower wavenumbers occurs as a result of 'phonon softening,' induced by the inclusion of boron within the diamond lattice. [21].

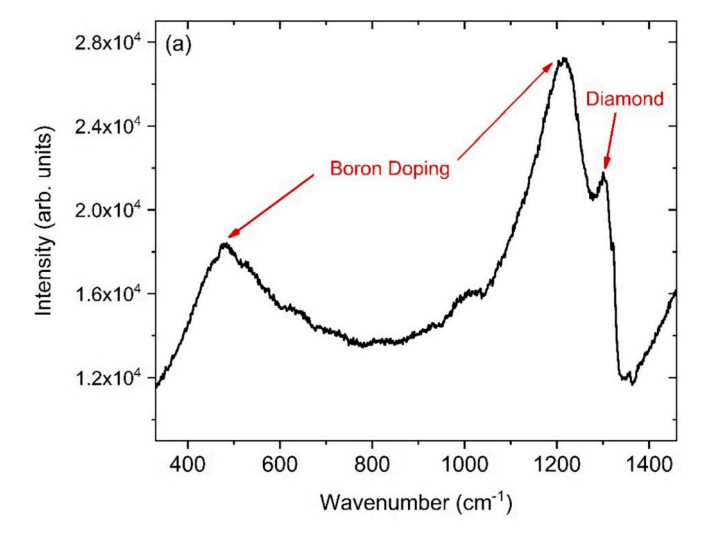


Fig. 4. Raman spectra of borocarbonitride $(B_x C_y N_z)$ coating in the 300–1500 \mbox{cm}^{-1} range.

3.5. Photoluminescence spectroscopy of borocarbonitride $(B_x C_y N_z)$

Fig. 5 shows the photoluminescence spectrum of the borocarbonitride $(B_xC_yN_z)$ coating excited by a 532 nm laser. The peaks at 575 nm and 625 nm are clearly observed in the spectra and correspond to neutral and negatively charged nitrogen vacancy emissions (NV 0 and NV $^-$, respectively) [27,34].

3.6. X-ray diffraction of boron carbonitride $(B_xC_yN_z)$

X-ray diffraction (XRD) analysis was employed to explore the crystal structure and phase composition of the coating, as depicted in Fig. 6(a). A close alignment with the theoretical pattern suggests a strong agreement between the experimental and theoretical diffraction patterns. Rietveld refinement revealed a mixed-phase structure, primarily consisting of BC₁₀N (81.9 %) and a secondary phase, BC₂N (18.1 %). The lattice parameters of the BC₁₀N phase were determined from the XRD data. The measured values, a = 2.528 Å, b = 2.532 Å, and c = 12.453 Å, closely matched the theoretically calculated values of a = 2.533 Å, b = 2.533 Å, and c = 12.453 Å.

This agreement between measured and calculated lattice parameters further validates the XRD analysis and confirms the crystalline structure of the BC $_{10}$ N phase in the synthesized coating. Fig. 6(b) highlights the most intense peak (c.a. 43.7 2-theta), which aligns closely with the corresponding peak in the theoretical XRD pattern of BC $_{10}$ N. This agreement indicates a good match between the experimental and theoretical data, suggesting that the coating predominantly consists of the BC $_{10}$ N phase.

3.7. Nanoindentation of borocarbonitride $(B_xC_yN_z)$

Fig. 7(a) illustrates the nanoindentation hardness results for the borocarbonitride $(B_xC_yN_z)$ coating. The indentation tests were conducted to a depth of 300 nm at multiple locations (N=10 indents) across the coating. The average hardness is determined to be 63 GPa, with nine measurements surpassing 40 GPa. The highest recorded hardness from an individual indent reached 111 GPa. The potential formation of nanotwinned $BC_{10}N$ could elucidate the observed hardness measurement exceeding 100 Gpa [35–37]. The $B_xC_yN_z$ sample has average Young's modulus of 802 GPa. In Fig. 7(b), the load-displacement curve of the indentation resulting in a hardness measurement of 90 GPa and a Young's modulus of 1190 GPa is depicted. Analyzing the ultimate unloading depth of the load-displacement curves enables the determination of the proportionate contributions of elastic and plastic deformation. A significant elastic recovery (approximately 75 %) is observed

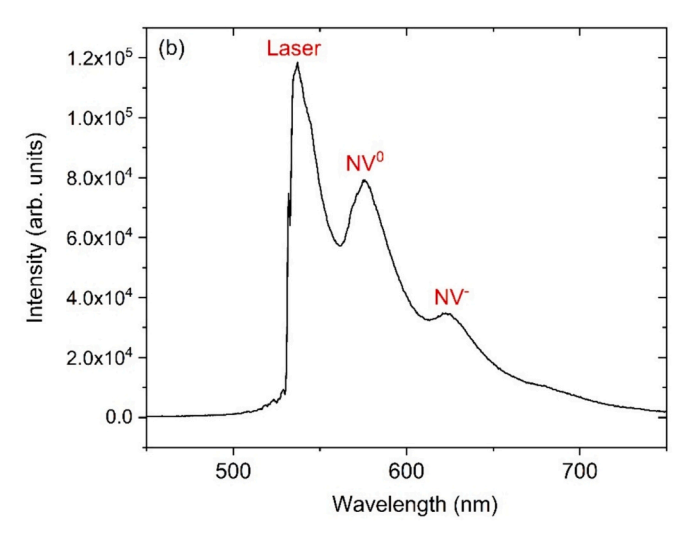


Fig. 5. Photoluminescence spectroscopy of B_xC_vN_z coating.

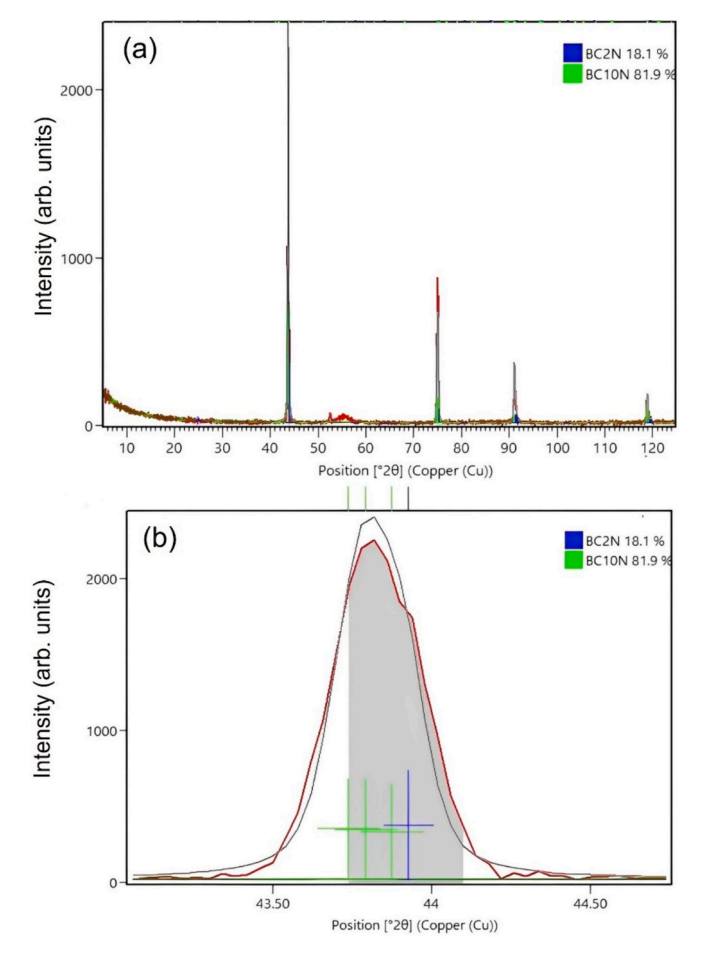
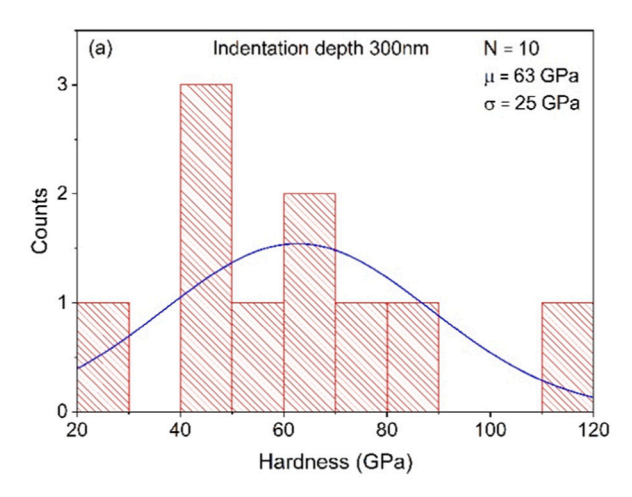


Fig. 6. (a) Experimental XRD pattern showing the mixed phase of $BC_{10}N$ (81.9%) and BC_2N (18.1%) by Rietveld refinement. (b) The most intense peak of the experimental XRD pattern matches well with the theoretical XRD pattern of $BC_{10}N$.

from the $B_xC_yN_z$ coating, as evidenced by the unloading data. Fig. 7(a) illustrates a notable variation in hardness data for $B_xC_yN_z$ coating. Possible factors contributing to this variability include the surface roughness of the sample and non-uniformity in material properties at the nanoindentation scale.

4. Discussions

The properties and the stoichiometry of coatings are strongly influenced by the deposition process and the gas phase chemistry in the system. In the case of borocarbonitride (BxCvNz) coatings, these characteristics are determined by factors such as the specific deposition process and the dissociation behavior of precursor molecules like B2H6 (diborane) and CH₄ (methane) into atomic boron, BH radicals, and C₂ radicals. When it comes to microwave plasma chemical vapor deposition (MPCVD), microwave power plays a crucial role in the dissociation of precursor molecules. Higher microwave power generally results in increased dissociation rates due to the greater energy input into the plasma. This dissociation behavior has been confirmed through optical emission spectroscopy (OES) measurements [38]. Our previous work demonstrated that copious amounts of atomic boron in the plasma at higher microwave power and lower pressure proves advantageous under certain growth conditions in the production of superhard boron-rich boron carbides [22]. OES measurements in this work have demonstrated that, with increasing microwave power, the dissociation of CH₄ into C₂ radicals becomes more pronounced. The increase in microwave power generally leads to higher plasma densities. The elevated plasma density provides a larger number of reactive species, promoting more collisions and interactions between species. This can contribute to the increased generation and accumulation of C2 emission. The rise in C2 peak intensity as chamber pressure increases is a result of the increased dissociation and decomposition of carbon-containing precursor gases such as methane (CH₄). As the chamber pressure increases, a higher concentration of precursor gas molecules leads to more collisions and interactions within the plasma. This increased density of precursor species promotes the dissociation of CH₄ into reactive carbon species, including C2 radicals. Consequently, the abundance of C2 radicals in the plasma increases. The C2 peak intensity increases until 80 Torr and then saturates in the range 80-100 Torr. The increased gas density in higherpressure environments leads to more frequent collisions between precursor species and other gas-phase species. These collisions can result in recombination reactions, where atoms or molecules combine to form different species. Therefore, other chemical species can be generated at a higher-pressure environment along with excited C2 radical. As a result, the generation of C2 radical saturates at an upper limit (80 Torr under our conditions) and other chemical species can be created at higher chamber pressure. However, these species may not be in an excited states and therefore would not be detectable by OES. The enhanced dissociation of CH₄ under higher microwave power and pressure conditions has implications for the deposition process and the resulting coating properties. The presence of atomic boron, BH radicals, and C2



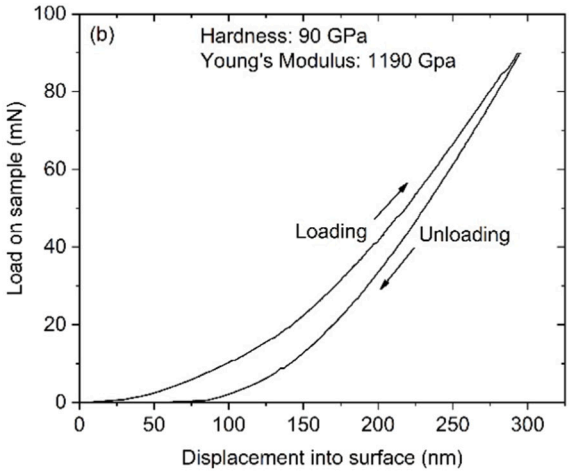


Fig. 7. (a) Histogram representing data from 10 indents, displaying the mean hardness value for the borocarbonitride coating, with numerous measurements exceeding 60 GPa. (b) Nanoindentation load-displacement curve obtained from a single location, revealing a hardness of 90 GPa at a depth of 300 nm.

radicals in the plasma contributes to the chemical reactions involved in the formation of $B_x C_y N_z$ coatings. These reactive species can react with other gas-phase species, such as carbon-containing and nitrogen-containing precursors, leading to the incorporation of carbon, nitrogen, and boron into the growing coating. The increased dissociation of $B_2 H_6$ and $C H_4$ under higher microwave power conditions can also impact the stoichiometry, composition, and properties of the $B_x C_y N_z$ coatings. More atomic boron, BH radicals, and C_2 radicals allow for greater incorporation of boron, carbon, and nitrogen into the coating, influencing the boron-to-carbon, boron-to-nitrogen, and carbon-to-nitrogen ratios. In our experiments, optimum experimental conditions were found for $B C_{10} N$ growth by analyzing the OES spectra of feedgas mixtures.

The generalized mechanism for the microwave plasma CVD synthesis of novel BC₁₀N involves the use of reactive gases CH₄, B₂H₆, and N₂ within a hydrogen-rich plasma. Microwave power dissociate the gas molecules and generates reactive species, including atomic hydrogen, atomic boron, BH, N2, C2, CN, and others in the plasma. The operating chamber pressures, microwave power, and gas flow rates were optimized based on optical emission spectroscopy studies. The synthesis was conducted at a microwave power of 1.6 kW and a fixed chamber pressure of 30 Torr. The gas flow rates were maintained at 500 Standard Cubic Centimeters per Minute (SCCM) of hydrogen, 25 SCCM of methane, 5 SCCM of nitrogen, and 5 SCCM of the diborane mixture. This specific ratio of gas flows, along with the set power and pressure conditions, proved ideal for the deposition of carbon-rich BC10N. The predominant hydrogen flow in the feedgas mixture produces a substantial amount of atomic hydrogen, which subsequently abstracts hydrogen from methane to form methyl radicals and dissociate other gas species in the plasma. Initially, the silicon substrate surface is terminated with atomic hydrogen. Vacant surface sites are created when the surface hydrogen atoms are abstracted by gas-phase hydrogen atoms to form H₂. Carbon, boron, and nitrogen-containing radicals are then transported to the surface through laminar, convective, and/or diffusive flow and adsorb onto the vacant sites. The formation energy of the predicted BC₁₀N is significantly lower than that of other predicted phases by Chen et al., such as B₄C₅N₃ and B₂C₃N, leading to the preferential formation of $BC_{10}N$ over other ternary BCN phases [21].

According to the XPS survey spectra, the synthesized borocarbonitride coating is composed of 82 % C, 9.5 % B, and 8.5 % N (rel. at.%) with no other elements present. The atomic percentage of carbon, boron and nitrogen yields a B/N ratio 1.1 and C/N ratio 9.6 and C/B ratio 8.6 which is closely matched to the stoichiometry of BC₁₀N. Hi-res C1s, B1s and N1s also confirms B—C, C—N, B—N and B-N-C bonding in the coating. FTIR also demonstrates C—C, B—C, B—N, C—N, and B-N-C peaks, which also suggests the synthesized coating is a ternary B-C-N structure.

Raman measurements conducted on the B_xC_vN_z coatings revealed interesting findings. The spectra exhibited distinct peaks related to boron doping as well as the characteristic diamond peak, which appeared at a wavenumber of 1305 cm⁻¹ (significantly lower than the unperturbed zone-center optical phonon at 1332 cm⁻¹). This shift in the diamond peak position indicates the presence of boron atoms in the lattice, which can induce structural modifications and affect the mechanical and electronic properties of the coatings. Furthermore, the Raman results suggested that the phonon bands in the B_xC_vN_z coatings become 'softened' as the boron-to-nitrogen (B/N) content increases [21]. The softening of phonon bands is an intriguing phenomenon that indicates changes in the vibrational characteristics of the material. This softening may arise from the incorporation of boron and nitrogen atoms in the lattice [21]. In addition to the Raman measurements, photoluminescence (PL) measurements were conducted to gain further insights into the B_xC_vN_z coatings. The PL spectra revealed the presence of nitrogen centers within the coatings. The identification of nitrogen centers through photoluminescence measurements further confirms the presence of substitutional nitrogen in the coating.

Experimental X-ray diffraction (XRD) data obtained from the synthesized coating was evaluated using Rietveld refinement analysis. The results of the refinement revealed an excellent agreement between the experimental XRD pattern and the theoretical XRD pattern of BC10N. The Rietveld refinement analysis also provided insights into the phase composition of the synthesized coating. The coating is predominantly comprising of the BC10N phase, accounting for approximately 81.9 % of the material. Additionally, another phase, BC₂N, was detected in the coating, comprising approximately 18.1 % of the material. The experimental XRD data, in conjunction with the Rietveld refinement analysis, provide valuable insights into the coating's crystal structure and phase composition. The close alignment between the experimental and theoretical diffraction patterns and the agreement in lattice parameters supports the identification of BC10N as the predominant phase in the coating. The presence of both BC10N and BC2N phases suggests a mixed composition, highlighting the complexity and diversity of the synthesized B_xC_vN_z material.

The synthesized coating exhibited impressive mechanical properties, as demonstrated by nanoindentation hardness measurements. The hardness values obtained from the measurements indicate that the coating falls within the superhard regime (i.e. > 40 GPa). The average Young's modulus of this sample is 802 GPa and average hardness is 63 GPa with standard deviation of 25 GPa. The spread observed in the nanoindentation hardness measurements, can be influenced by several factors. Two significant factors that may contribute to this variation include the roughness of the sample surface and the non-uniformity in material properties at the nanoindentation scale. When the indenter contacts a rough surface, the effective contact area may vary, leading to variations in the measured hardness values. Surface roughness can cause fluctuations in the applied load and affect the deformation behavior during indentation, resulting in different hardness measurements across the sample [39,40]. Furthermore, non-uniformity in material properties at the nanoindentation scale can also contribute to the dispersion observed in hardness values. Even in a relatively uniform coating, there can be inherent variations in the microstructure or composition that can impact the mechanical response. Variations in grain size and chemical composition can influence the local mechanical properties and lead to differences in hardness measurements.

5. Conclusions

This work describes the first successful effort in synthesizing theoretically-predicted BC₁₀N by MPCVD. According to XPS survey spectra, the boron carbonitride coating is composed of 82 % C, 9.5 % B, and 8.5 % N (rel. at.%), which is closely matched to the stoichiometry of BC₁₀N. XPS and FTIR also confirm B—C, C—N, B—N, and B-N-C bonding in the synthesized coating. Raman measurements showed evidence of boron doping, and photoluminescence measurements confirmed the presence of nitrogen centers. The XRD patterns were analyzed by Rietveld refinement to show that the coating is composed of BC10N as the major phase, accounting for approximately 81.9 % of the total composition. A secondary phase of BC2N is also present, constituting approximately 18.1 % of the coating. The nanoindentation hardness measurement of synthesized coating is in a superhard regime with an average hardness of 63 GPa. CVD synthesis of this novel superhard BC₁₀N material paves the way for a wide range of potential applications in refractories, medical systems, fast-breeders, lightweight armors, ballistic armors, cutting tools, high-temperature thermoelectric conversion systems, and many more.

CRediT authorship contribution statement

Kallol Chakrabarty: Writing – original draft, Methodology, Investigation, Formal analysis, Data curation. Paul A. Baker: Investigation. Shane A. Catledge: Writing – review & editing, Supervision, Project administration, Funding acquisition, Conceptualization.

Declaration of competing interest

The authors declare that they have no known competing financial interests or personal relationships that could have appeared to influence the work reported in this paper.

Data availability

The data that support the findings of this study are available from the corresponding author upon reasonable request.

Acknowledgments

This work is supported by the NSF EPSCoR RII-Track-1 Cooperative Agreement OIA-2148653. This research was supported in part by the Alabama State funded Graduate Research Scholars Program (GRSP). Any opinions, findings, and conclusions or recommendations expressed in this material are those of the author and do not necessarily reflect the views of the National Science Foundation.

References

- [1] S. Chen, X.G. Gong, S.-H. Wei, Phys. Rev. B 77 (2008).
- [2] Y.M.C. Wenjun Zhang, Bin He, I. Bello, Shuit-Tong Lee, Comprehensive Hard Materials. 2014. p. 33.
- [3] R.S. Balmer, J.R. Brandon, S.L. Clewes, H.K. Dhillon, J.M. Dodson, I. Friel, P. N. Inglis, T.D. Madgwick, M.L. Markham, T.P. Mollart, N. Perkins, G.A. Scarsbrook, D.J. Twitchen, A.J. Whitehead, J.J. Wilman, S.M. Woollard, J. Phys. Condens. Matter 21 (2009) 364221.
- [4] J.E. Field, Rep. Prog. Phys. 75 (2012) 126505.
- [5] S.D. Nehate, A.K. Saikumar, A. Prakash, K.B. Sundaram, Mater. Today Adv. 8 (2020) 100106.
- [6] C.B. Samantaray, R.N. Singh, Int. Mater. Rev. 50 (2013) 313-344.
- [7] A.K. Suri, C. Subramanian, J.K. Sonber, T.S.R.C. Murthy, Int. Mater. Rev. 55 (2013) 4-40.
- [8] J. Wöhle, H. Ahn, K.T. Rie, Surf. Coat. Technol. 116-119 (1999) 1166-1171.
- [9] V.S. Sulyaeva, M.L. Kosinova, Y.M. Rumyantsev, F.A. Kuznetsov, V.G. Kesler, V. V. Kirienko, Thin Solid Films 558 (2014) 112–117.
- [10] Y. Wada, Y.K. Yap, M. Yoshimura, Y. Mori, T. Sasaki, Diamond Relat. Mater. 9 (2000) 620–624.
- [11] J.L. Xiao, C.B. Wang, Q. Shen, L.M. Zhang, Surf. Coat. Technol. 276 (2015) 141–144.

- [12] W.R. Matizamhuka, I. Sigalas, M. Herrmann, L. Dubronvinsky, N. Dubrovinskaia, N. Miyajima, G. Mera, R. Riedel, Materials (Basel) 4 (2011) 2061–2072.
- 13] T. Tavsanoglu, M. Jeandin, O. Addemir, Surf. Eng. 32 (2016) 755-760.
- [14] J. Lü, H. Li, P. Zhu, X. Lü, Y. Li, Appl. Surf. Sci. 257 (2011) 4963-4967
- [15] Y. Zhao, D.W. He, L.L. Daemen, T.D. Shen, R.B. Schwarz, Y. Zhu, D.L. Bish, J. Huang, J. Zhang, G. Shen, J. Qian, T.W. Zerda, J. Mater. Res. 17 (2011) 3139–3145.
- [16] V.P. Filonenko, V.N. Khabashesku, V.A. Davydov, I.P. Zibrov, V.N. Agafonov, Inorg. Mater. 44 (2011) 395–400.
- [17] M. Hubáček, T. Sato, J. Solid State Chem. 114 (1995) 258-264.
- [18] I. Shimoyama, Y. Baba, T. Sekiguchi, Carbon 71 (2014) 1-10.
- [19] V. Linss, I. Hermann, N. Schwarzer, U. Kreissig, F. Richter, Surf. Coat. Technol. 163-164 (2003) 220–226.
- [20] S. Xu, X. Ma, G. Tang, Q. Zhang, Surf. Eng. 31 (2015) 549-555.
- [21] W.-C. Chen, J.N. Schmidt, D. Yan, Y.K. Vohra, C.-C. Chen, npj Comput. Mater. 7 (2021).
- [22] K. Chakrabarty, W.C. Chen, P.A. Baker, V.M. Vijayan, C.C. Chen, S.A. Catledge, Materials (Basel) 13 (2020).
- [23] B. Ramkorun, K. Chakrabarty, S.A. Catledge, Mater. Res. Express 8 (2021).
- [24] M.A. Mannan, H. Noguchi, T. Kida, M. Nagano, N. Hirao, Y. Baba, Mater. Sci. Semicond. Process. 11 (2008) 100–105.
- [25] M.A. Mannan, M. Nagano, N. Hirao, Y. Baba, Chem. Lett. 37 (2008) 96-97.
- [26] F. Zhou, Q. Wang, B. Yue, X. Wu, L. Zhuge, X. Cheng, Mater. Chem. Phys. 138 (2013) 215–224.
- [27] D.Y. Liu, L.C. Hao, Y. Teng, F. Qin, Y. Shen, K. Tang, J.D. Ye, S.M. Zhu, R. Zhang, Y. D. Zheng, S.L. Gu, APL Mater. 9 (2021).
- [28] T. Sugiyama, T. Tai, T. Sugino, Appl. Phys. Lett. 80 (2002) 4214-4216.
- [29] V.S. Sulyaeva, M.L. Kosinova, Y.M. Rumyantsev, V.G. Kesler, F.A. Kuznetsov, Surf. Coat. Technol. 230 (2013) 145–151.
- [30] B. Singh, G. Kaur, P. Singh, K. Singh, B. Kumar, A. Vij, M. Kumar, R. Bala, R. Meena, A. Singh, A. Thakur, A. Kumar, Sci. Rep. 6 (2016) 35535.
- [31] J. Li, X. Xiao, X. Xu, J. Lin, Y. Huang, Y. Xue, P. Jin, J. Zou, C. Tang, Sci. Rep. 3 (2013) 3208.
- [32] X.-Y. Miao, H.-A. Ma, Z.-F. Zhang, L.-C. Chen, L.-J. Zhou, M.-S. Li, X.-P. Jia, Chin. Phys. B 30 (2021) 068102.
- [33] V. Mortet, A. Taylor, Z. Vlčková Živcová, D. Machon, O. Frank, P. Hubík, D. Tremouilles, L. Kavan, Diamond Relat. Mater. 88 (2018) 163–166.
- [34] Q. Liang, C.Y. Chin, J. Lai, C.-S. Yan, Y. Meng, H.-K. Mao, R.J. Hemley, Appl. Phys. Lett. 94 (2009).
- [35] Q. Huang, D. Yu, B. Xu, W. Hu, Y. Ma, Y. Wang, Z. Zhao, B. Wen, J. He, Z. Liu, Y. Tian, Nature 510 (2014) 250–253.
- [36] Y. Tian, Nature 510 (2014) 250-253.
 [37] Y. Tian, B. Xu, D. Yu, Y. Ma, Y. Wang, Y. Jiang, W. Hu, C. Tang, Y. Gao, K. Luo,
- Z. Zhao, L.M. Wang, B. Wen, J. He, Z. Liu, Nature 493 (2013) 385–388.
 [37] B. Yang, X. Peng, C. Huang, Z. Wang, D. Yin, T. Fu, Carbon 150 (2019) 1–7.
- [38] K. Chakrabarty, I. Arnold, S.A. Catledge, J. Vac. Sci. Technol. A 37 (2019).
- [39] W.-G. Jiang, J.-J. Su, X.-Q. Feng, Eng. Fract. Mech. 75 (2008) 4965–4972.
- [40] M. Laurent-Brocq, E. Bejanin, Y. Champion, Scanning 37 (2015) 350-360.